X-ray Study of CSO NGC 3894

Karthik Balasubramaniam[1] (karthik@oa.uj.edu.pl)
PhD scholar

Collaborators : Ł. Stawarz[1] , V. Marchenko[1] , M. Sobolewska[2] , A. Siemiginowska[2] , C.C. Cheung[3], D. Król[1]

[1]**Astronomical observatory, Jagiellonian university-Krakow, Poland**

[2]*Harvard Smithsonian Center for Astrophysics, USA*

[3]*Space Science Division, Naval Research Laboratory, USA*

6th CSSGPS workshop

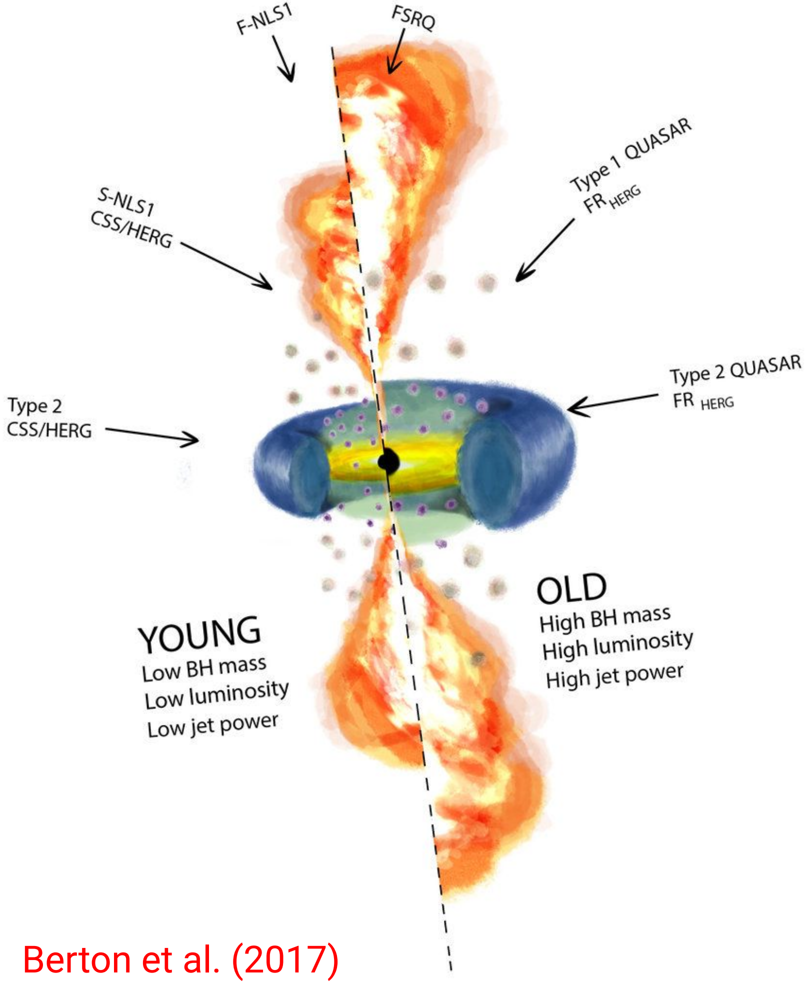

Berton et al. (2017)

An orientation/evolutionary-based unification of jetted active galactic nuclei.

Unification scheme of jetted-AGN with high accretion rate with respect to the Eddington limit and a high-density photon-rich environment. On the left side, young and smaller sources (NLS1s and CSS sources), compared to older and larger objects (FSRQs and FR HERG)

- Compact symmetric objects (CSOs) are jetted active galactic nuclei (AGNs) with a double-lobed radio structure confined to within 1 kpc.
- CSOs represent the earliest evolutionary phase of jetted AGNs. Some of them may eventually evolve into large-scale extended double sources, while others stall within the host galaxy and die out, depending on the longevity of nuclear activity, the jet power, and parameters of the surrounding galactic environment.
- Studying CSOs enables us to understand the evolution of galaxies and the interactions between relativistic jets and the interstellar medium of the hosts.

Optical Host

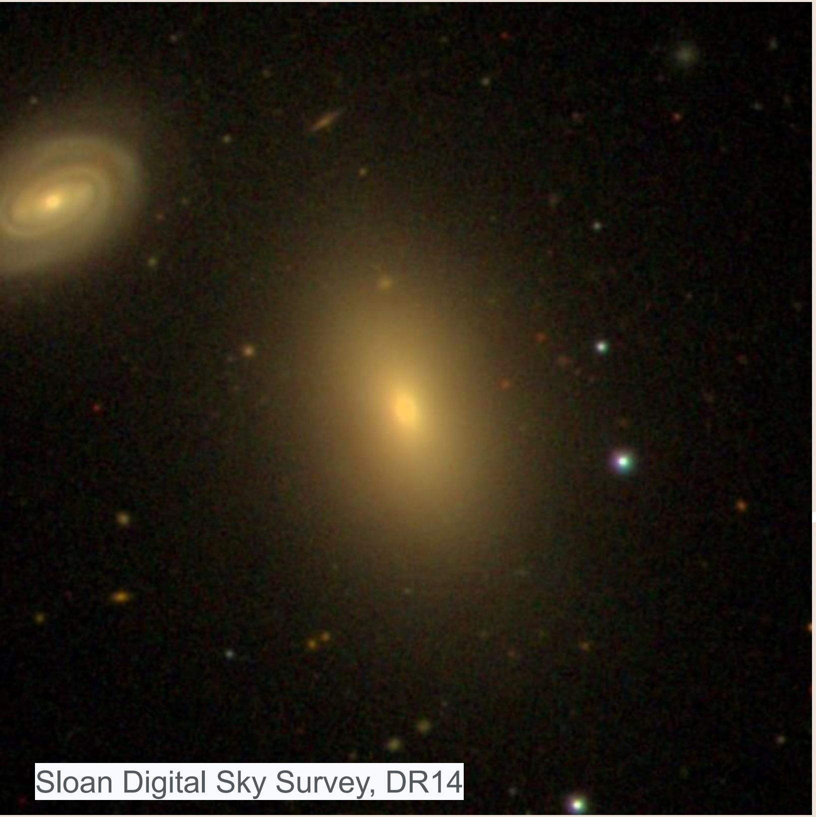

Sloan Digital Sky Survey, DR14

2MASS All Sky Survey

NGC 3894 / TXS 1146+596

- Bright nearby E/S0 galaxy discovered already by William Herschel
- Luminosity Distance = 50.1Mpc
- Scale = 0.24 kpc/arcsec
- Hubble Space Telescope observations of NGC 3894: see Perlman et al. 2001

RA: 11h 48m 50.3582s
Dec: +59d 24m 56.382s

Compact Radio Structure

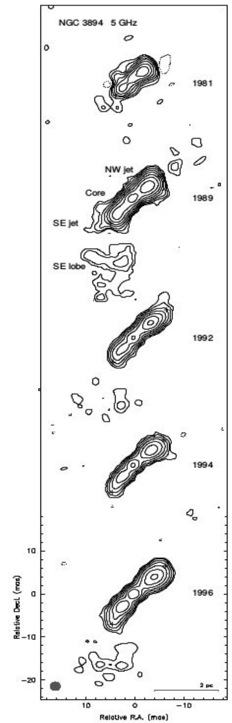

FIG. 1.—Time montage of CLEANed VLBI images of NGC 3894 at 5.0 GHz from 1981 to 1996. The synthesized restoring beam for each image has a FWHM of 2 mas (0.31 h^{-1} pc) and is drawn in the lower left-hand corner of the montage. Contours are drawn logarithmically at a factor of 2 intervals, with the first positive contour at 2, 0.5, 2, 2, and 1 mJy beam^{-1} for epochs 1981–1996, respectively. The crosses mark the northwest and southeast edges of the source at the 8 mJy beam^{-1} level. Component labels are the same as for Table 2.

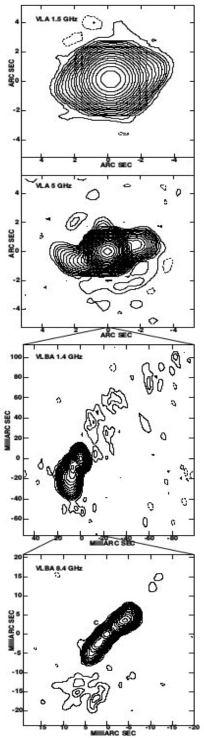

FIG. 2.—Angle montage of CLEANed images of NGC 3894 from arcsecond to mas scales. The restoring beam is 1.8, 1, 0.01 × 0.005 in position angle 10°, and 0″.002 going from top to bottom. Contours are drawn at 660, 57, 350, and 650 μJy beam^{-1} × (−2, −1, 1, 2, 3, 4, 5.6, 6, 8, etc., increasing by root 2) in the images from top to bottom, respectively. The component labeled "C" in the VLBA image at 8.4 GHz is identified as the core.

- 1146+596 recognized as a compact radio source by Condon & Dressel (1978);
- First VLBI imaging at 5 GHz (Wrobel et al. 1985) suggested the presence of three radio components, consistent with an asymmetric core-jet structure;
- The VLBI 1981-1996 monitoring analyzed by Taylor et al. (1998) indicated that the twin jets were mildly relativistic with velocities v~0.3 c and oriented at ~50deg from the line-of-sight.

Compact Radio Structure

Most recently, Principe et al. (2020) claimed that "VLBA results favor the youth scenario for the inner structure of this object, with an estimated dynamical age of 59 +/- 5 years, and the jet viewing angle 10-20deg"

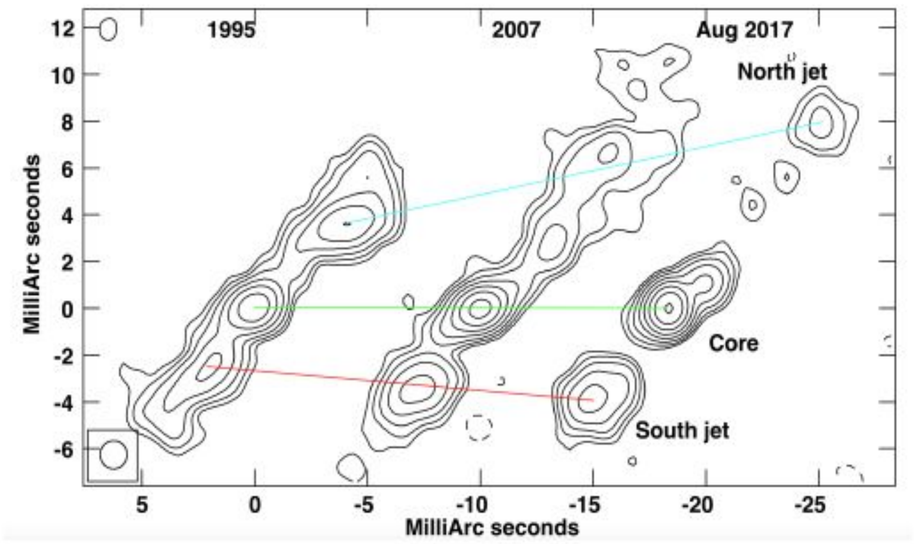

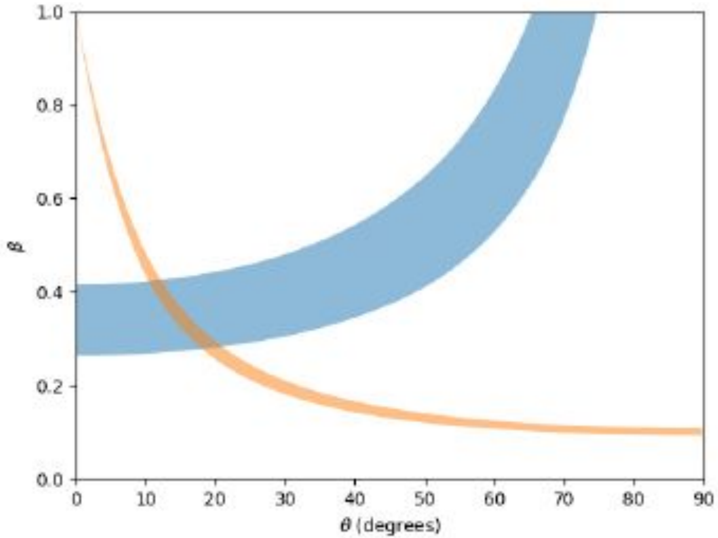

Compact Radio Structure

“The 21 cm atomic hydrogen line is seen in absorption slightly redshifted with respect to the systemic velocity toward the core, jet, and counterjet of this source. There are four components in the gas that are spatially and/or spectrally distinct, two of which appear to be part of a single larger structure, possibly a circumnuclear torus.” (Peck & Taylor 1998, Gupta et al. 2006)

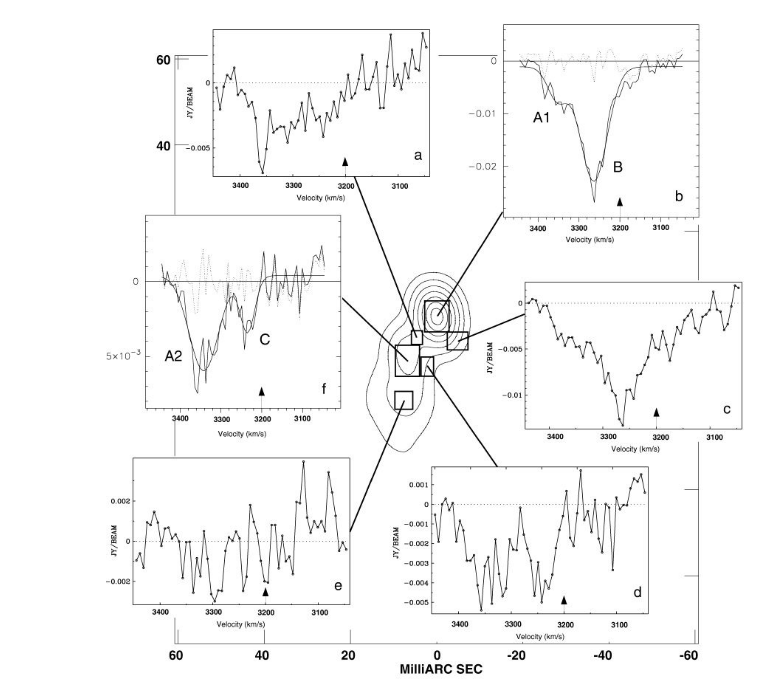

IR Observations

MIR studies (IRAS, Spitzer, WISE) indicate the low-luminosity LINER-type AGN, and low star formation rate ~0.5 M_{sol}/yr in the host

(Willett et al. 2010, Kosmaczewski et al. 2020)

Table 1
MIR Properties of X-Ray-detected CSOs

Name (1)	z (2)	d_L (Mpc) (3)	LS (pc) (4)	Class (5)	$W1-W2$ (mag) (6)	$W2-W3$ (mag) (7)	WISE color (8)	IRAS $L_{12\,\mu m}$ (10^{43} erg s^{-1}) (9)	MIPS $L_{24\,\mu m}$ (10^{43} erg s^{-1}) (10)	WISE $L_{12\,\mu m}$ (10^{43} erg s^{-1}) (11)	$L_{2-10\,keV}$ (10^{43} erg s^{-1}) (12)	Reference (13)
0019–000	0.305	1521	220	GPS	0.472	2.441	G	···	···	3.53 ± 0.11	0.55^	T09
0026+346	0.517	2852	190	GPS	0.743	2.491	Un	···	···	21 ± 0.3	23 ± 2	G06
0035+227	0.096	418	21.8	CSO	0.148	1.265	G	···	···	0.425 ± 0.007	0.075 ± 0.034	S16
0108+388	0.669	3907	22.7	CSO	0.132	3.159	G	9.86 ± 9.16	3.79 ± 1.40	<13.1	7 ± 3	T09,S16
0116+319	0.059	255	70.1	CSO	0.035	1.682	S*	0.595 ± 0.056	0.609 ± 0.046	0.629 ± 0.003	<0.10†	S16
0402+379	0.055	234	7.3	CSO	0.099	1.721	G	0.48 ± 0.07	0.949 ± 0.059	0.608 ± 0.004	0.041 ± 0.016	R14
0428+205	0.219	1044	653	GPS	0.323	2.648	G	···	···	3.93 ± 0.08	1.4 ± 0.6	T09
0500+019	0.585	3319	55	GPS	1.047	2.892	Q	63.4 ± 6.5	87.2 ± 9.8	59.3 ± 0.5	50 ± 6	T09
0710+439	0.518	2868	87.7	CSO	0.726	2.997	Sy	43.8 ± 4.4	107 ± 7	43.4 ± 0.4	39.40 ± 3.15	T09,S16
0941–080	0.228	1100	148	GPS	0.388	2.444	G*	···	···	2.57 ± 0.05	0.091 ± 0.075	T09
1031+567	0.460	2480	109	CSO	0.999	2.922	Q	17.6 ± 3.0	16.5 ± 4.7	15.6 ± 0.3	2.2 ± 0.2	T09,S16
1117+146	0.362	1874	306	GPS	0.406	3.599	SB	···	···	<5.87	1.40 ± 0.19	T09
1146+596	0.011	47	933	CSO	–0.011	1.237	G	0.0816 ± 0.0022	0.0818 ± 0.0033	0.1010 ± 0.0002	0.007	U05
1245+676	0.107	478	9.6	CSO	0.130	1.409	G	0.33 ± 0.14	0.358 ± 0.098	0.531 ± 0.006	0.031††	W09,S16
1323+321	0.368	1908	247	GPS	0.303	2.014	G	···	···	2.54 ± 0.11	3.7 ± 0.4	T09
1345+125	0.122	551	166	CSO	1.308	3.930	Sy*	83.3 ± 1.7	216 ± 4	87.9 ± 0.2	7.8 ± 1.5	T09,J13
1358+624	0.431	2298	218	GPS	1.210	2.592	Q*	31.0 ± 2.4	37.8 ± 2.8	35.4 ± 0.2	30 ± 20	T09
1404+286	0.077	336	10.0	CSO	1.018	3.063	Q	50.9 ± 0.9	65.2 ± 1.3	51.6 ± 0.1	0.45 ± 0.06^C	T09,S16,S19b
1511+0518	0.084	370	7.3	CSO	1.233	2.899	Q	···	51.1 ± 3	52.2 ± 0.1	3^C	S16
1607+268	0.473	2569	240	CSO	0.287	2.679	S*	4.21 ± 3.17	21.6 ± 4.4	<7.27	3.79 ± 0.87	T09,S16
1718–649	0.014	60.4	2.0	CSO	0.136	2.462	G	0.322 ± 0.009	0.32 ± 0.01	0.401 ± 0.001	0.0154 ± 0.0024	S16
1843+356	0.763	4612	22.3	CSO	1.160	4.047	Sy	···	···	190 ± 1	5.60 ± 2.28	S16
1934–638	0.183	845	85.1	CSO	0.609	3.360	Sy*	5.89 ± 0.62	19 ± 1	6.52 ± 0.03	0.60 ± 0.14	S16,S19a
1943+546	0.263	1285	107.1	CSO	0.628	2.191	Un	···	···	5.64 ± 0.04	0.73 ± 0.28	S16
1946+708	0.101	444	39.4	CSO	0.663	2.336	Un	1.75 ± 0.15	1.67 ± 0.10	1.69 ± 0.01	1.20 ± 0.18	S16,S19a
2008–068	0.547	3056	218	CSO	0.334	2.159	G	···	7.68 ± 0.35	9.1 ± 0.4	6 ± 2	T09
2021+614	0.227	1086	16.1	CSO	1.287	3.009	Q	<210	···	64.9 ± 0.2	11.2^C	S16,S19a
2128+048	0.990	6364	218	GPS	0.688	3.352	Sy	···	63.9 ± 2.3	<52.4	29 ± 4	T09
2352+495	0.238	1143	117.3	CSO	0.688	2.714	Sy	···	···	4.25 ± 0.04	1.3 ± 0.3	T09,S16

Note. Column (1): name of the source. Column (2): redshift. Column (3): luminosity distance. Column (4): linear size of the radio lobes taken from the references provided in Column (13), except for 1146+596, cited from Perlman et al. (2001). Column (5): morphological/spectral radio classification: CSO based on the radio morphology, GPS based on the spectral classification; classification follows the references given in Column (13), except for 1146+596, following from Perlman et al. (2001). Column (6): WISE difference in the $W1$ (3.4 μm) and $W2$ (4.6 μm) color bands. Column (7): WISE difference in the $W2$ (4.6 μm) and $W3$ (12 μm) color bands. Column (8): color classification: "Galaxy" (G), "Starburst" (SB), Quasar/Seyfert (Q/Sy), "Uncertain" (Un); possible contamination of WISE fluxes by background/foreground sources denoted by a star. Column (9): IRAS 12 μm luminosity. Column (10): Spitzer/MIPS 24 μm luminosity. Column (11): WISE 12 μm luminosity calculated from the $W3$ band magnitude. Column (12): unabsorbed 2 – 10 keV luminosity taken from the references provided in Column (13); ^ extrapolated from the detection in the 0.5–2 keV band with photon index =1.61; † estimated from the 0.5–2.0 keV upper limit $<0.5 \times 10^{-14}$ erg cm^{-2} s^{-1} assuming photon index =2.0; †† calculated based on the 4.5–12.0 keV PN flux; ^{C} value corresponding to the "Compton-thick" scenario. Column (13): X-ray references: Guainazzi et al. (2006) (G06), Jia et al. (2013) (J13), Romani et al. (2014) (R14), Siemiginowska et al. (2016) (S16), Sobolewska et al. (2019a) (S19a), Sobolewska et al. (2019b) (S19b), Tengstrand et al. (2009) (T09), Ueda et al. (2005) (U05), Watson et al. (2009) (W09).

Table 7
Derived mid-IR Properties of the CSO Sample

Object	SFR_{Ne} ($M_\odot$ yr^{-1})	SFR_{PAH} ($M_\odot$ yr^{-1})	A_V (mag)	$T_{H_2}^{warm}$ (K)	$M_{H_2}^{warm}$ ($10^7\,M_\odot$)	$T_{H_2}^{hot}$ (K)	$M_{H_2}^{hot}$ ($10^7\,M_\odot$)	T_{dust} (K)	log M_{BH}^{OIV} ($M_\odot$)	log M_{BH}^{bulge} ($M_\odot$)
4C +31.04	7.8 ± 1.1	6.4	15 ± 6	338 ± 100	0.47 ± 0.13	...	...	65	<8.16	8.78
4C +37.11	17 ± 1	[0.8 – 1.6]	9 ± 3	354 ± 90	0.95 ± 0.05	854 ± 240	0.09 ± 0.02	...	<7.96	8.74
1146+59	0.5 ± 0.1	0.3	13 ± 1	537 ± 50	0.01 ± 0.002	...	...	150	9.23 ± 0.52	8.40
4C +12.50	159 ± 14	31.5	8 ± 0.6	326 ± 97	4.26 ± 0.46	...	...	85	...	8.81
OQ 208	54 ± 3	47.8	...	281 ± 101	1.13 ± 0.13	...	...	110	<7.79	8.81
PKS 1413+135	<150	<80	13 ± 0.4	...	...	...	...	90	...	8.22
PKS 1718–649	1.8 ± 0.1	0.8	7 ± 3	202 ± 112	0.12 ± 0.01	...	...	...	8.62 ± 0.45	8.48
1946+70	11.1 ± 0.9	[1.7 – 3.1]	11 ± 3	320 ± 83	0.74 ± 0.05	...	...	...	...	8.54

Gamma-ray Emission

A&A 635, A185 (2020)
https://doi.org/10.1051/0004-6361/201937049

Astronomy & Astrophysics

NGC 3894: a young radio galaxy seen by *Fermi*-LAT

G. Principe[1], G. Migliori[1,2], T. J. Johnson[3], F. D'Ammando[1], M. Giroletti[1], M. Orienti[1], C. Stanghellini[1], G. B. Taylor[4], E. Torresi[5], and C. C. Cheung[6]

[1] INAF – Istituto di Radioastronomia, Bologna, Italy
e-mail: giacomo.principe@inaf.it
[2] Dip. di Fisica e Astronomia, Università di Bologna, Bologna, Italy
[3] College of Science, George Mason University, Resident at Naval Research Laboratory, Washington DC, USA
[4] University of New Mexico, Albuquerque, NM, USA
[5] INAF – Osservatorio di Astrofisica e Scienza dello Spazio di Bologna, Bologna, Italy
[6] Naval Research Laboratory, Space Science Division, Washington DC, USA

Received 4 November 2019 / Accepted 28 February 2020

ABSTRACT

Context. According to radiative models, radio galaxies may produce γ-ray emission from the first stages of their evolution. However, very few such galaxies have been detected by the *Fermi* Large Area Telescope (LAT) so far.
Aims. NGC 3894 is a nearby ($z = 0.0108$) object that belongs to the class of compact symmetric objects (CSOs, i.e., the most compact and youngest radio galaxies), which is associated with a γ-ray counterpart in the Fourth *Fermi*-LAT source catalog. Here we present a study of the source in the γ-ray and radio bands aimed at investigating its high-energy emission and assess its young nature.
Methods. We analyzed 10.8 years of *Fermi*-LAT data between 100 MeV and 300 GeV and determined the spectral and variability characteristics of the source. Multi-epoch very long baseline array (VLBA) observations between 5 and 15 GHz over a period of 35 years were used to study the radio morphology of NGC 3894 and its evolution.
Results. NGC 3894 is detected in γ-rays with a significance $>9\sigma$ over the full period, and no significant variability has been observed in the γ-ray flux on a yearly time-scale. The spectrum is modeled with a flat power law ($\Gamma = 2.0 \pm 0.1$) and a flux on the order of 2.2×10^{-9} ph cm^{-2} s^{-1}. For the first time, the VLBA data allow us to constrain with high precision the apparent velocity of the jet and counter-jet side to be $\beta_{\rm app,NW} = 0.132 \pm 0.004$ and $\beta_{\rm app,SE} = 0.065 \pm 0.003$, respectively.
Conclusions. *Fermi*-LAT and VLBA results favor the youth scenario for the inner structure of this object, with an estimated dynamical age of 59 ± 5 years. The estimated range of viewing angle ($10^\circ < \theta < 21^\circ$) does not exclude a possible jet-like origin of the γ-ray emission.

Key words. Galaxy: evolution – galaxies: nuclei – galaxies: general – galaxies: jets – radio continuum: galaxies – gamma-rays: galaxies

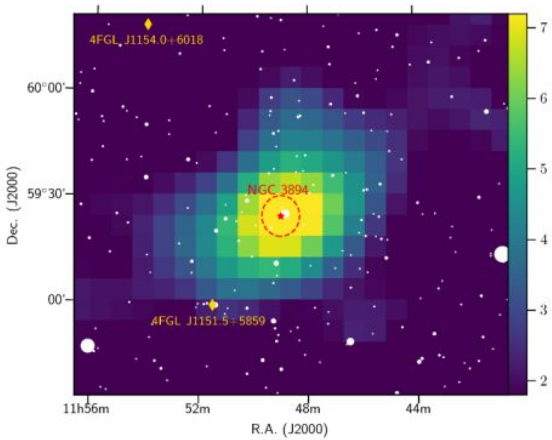

Fig. 1. *Fermi*-LAT TS map (in sigma units) above 3 GeV, the red star and dashed circle represent the central position and the 95% confidence-level uncertainty $R_{95} = 0.05^\circ$ of the γ-ray source, respectively. White dots show radio sources from the NVSS survey scaled depending on their flux.

Gamma-ray Emission

Table 6
Properties of Fermi-detected and Other Nearby CSO Galaxies

Source Name (1)	z (2)	D_L (Mpc) (3)	Host Galaxy (4)	Kiloparsec Morphology (5)	LLS (pc) (6)	θ (deg) (7)	β_{app} (c) (8)	Age (yr) (9)	ν_m (GHz) (10)	f (11)
Fermi-detected CSOs										
TXS 0128+554	0.036	159	Elliptical	C	12	52^{+7}_{-9}	0.32 ± 0.07	82 ± 17	0.66	0.48
NGC 3894	0.011	47	Elliptical	E	7	10–21	~0.1	59 ± 5	5	0.18
PKS 1718−649	0.014	62	Elliptical[a]	C	2.5	⋯	0.06 ± 0.03	70 ± 30	3.6	<0.01
PMN J1603−4904	0.232	1148	Unknown[b]	E	56	⋯	<3	>54	0.39	0.37
Low-redshift CSOs Lacking Fermi-LAT Associations										
4C 31.04	0.060	266	Elliptical	C	100	75–80	0.34	550	0.4	0.016
PMN J1511+0518	0.084	378	Elliptical	C	11	⋯	0.28	55	10	0.03
B2 0035+22	0.096	435	Elliptical	C	22	⋯	0.5	450	0.4–1.4	0.014

Notes. Columns are as follows: (1) source name, (2) redshift, (3) luminosity distance in Mpc, (4) host galaxy type, (5) kiloparsec-scale radio morphology, where E = extended, and C = compact, (6) largest projected linear size of inner jet structure as measured from hotspot-to-hotspot in parsecs, (7) jet viewing angle in degrees, (8) apparent expansion speed in units of the speed of light, (9) dynamical age of the radio source in years, (10) radio spectral turnover frequency in GHz, (11) ratio of core flux density to total flux density at 8 GHz.

[a] Host has an elliptical nucleus with a prominent dust lane, surrounded by faint spiral structure.

[b] No indications of active star formation in optical spectrum (Goldoni et al. 2016).

NGC 3894. This low-luminosity CSO is located in an elliptical galaxy at $z = 0.01075$, and was found to be γ-ray loud by Principe et al. (2020) after stacking 10.8 yr of Pass 8 Fermi-LAT data. The 5 GHz VLA image of Taylor et al. (1998) shows a bright core flanked by radio lobes separated by ~800 pc. On milliarcsecond scales, the flat-spectrum core is flanked by two bright, continuous jets with projected lengths of ~2 pc (Tremblay et al. 2016). Fainter diffuse emission is visible in both jets farther from the core in low-frequency VLBI images (Taylor et al. 1998). The inner radio source has a high core fraction ($f = 0.18$). Principe et al. (2020) find expansion speeds of ~0.1 c and a viewing angle of $10° \leqslant \theta < 21°$ for the inner jets. These measurements imply a young kinematic age of 59 ± 5 yr.

M.L. Lister et al 2020

Table 7
Spectral Properties of Fermi-detected and Other Nearby CSO Galaxies

Source Name (1)	log L_ν (1.4 GHz) (W Hz^{-1}) (2)	log νL_ν (0.5–2 keV) (erg s^{-1}) (3)	log νL_ν (2–10 keV) (erg s^{-1}) (4)	log νL_ν (0.1–100 GeV) (erg s^{-1}) (5)	Γ (0.1–100 GeV) (6)	log νL_ν (10–1000 GeV) (erg s^{-1}) (7)	Γ (10–1000 GeV) (8)
Fermi-detected CSOs							
TXS 0128+554	23.7	42.5	42.3	43.2	2.10 ± 0.09	42.5	3.1 ± 0.9
NGC 3894	23.1	40.5[a]	40.8	41.8	2.06 ± 0.12	⋯	⋯
PKS 1718−649	24.3	40.9	41.2	42.1	2.49 ± 0.18	⋯	⋯
PMN J1603−4904	26.3	43.5	43.6	45.9	2.02 ± 0.03	45.6	2.2 ± 0.10
Low-redshift CSOs Lacking Fermi-LAT Associations							
4C 31.04	25.3	<40.6	⋯	⋯	⋯	⋯	⋯
PMN J1511+0518	25.2	42.0	42.7	⋯	⋯	⋯	⋯
B2 0035+22	25.1	41.6	41.9	⋯	⋯	⋯	⋯

Note. Columns are as follows: (1) source name, (2) log of 1.4 GHz luminosity (L_ν) in W Hz^{-1}, (3) log of 0.5–2 keV x-ray luminosity in erg s^{-1}, (4) log of 2–10 keV x-ray luminosity (νL_ν) in erg s^{-1}, (5) log of 0.1–100 GeV γ-ray luminosity from 4FGL in erg s^{-1}, (6) 4FGL power-law photon index between 0.1 and 100 GeV, (7) log of 10–1000 GeV γ-ray luminosity from 3FHL in erg s^{-1}, (8) 3FHL power-law photon index between 10 and 1000 GeV.

[a] 0.7–2 keV luminosity.

Motivation

Well characterized at radio , IR , & optical frequencies

Archival Chandra Data (~40 ks) not analyzed (published) before!

One of the youngest nearby radio galaxies; one of a few CSOs detected in gamma-rays by Fermi-LAT!

A need for a proper X-ray spectroscopy and a broad-band SED

Archival Chandra Observation ~ 40 ks (PI : Perlman), not analyzed/published before

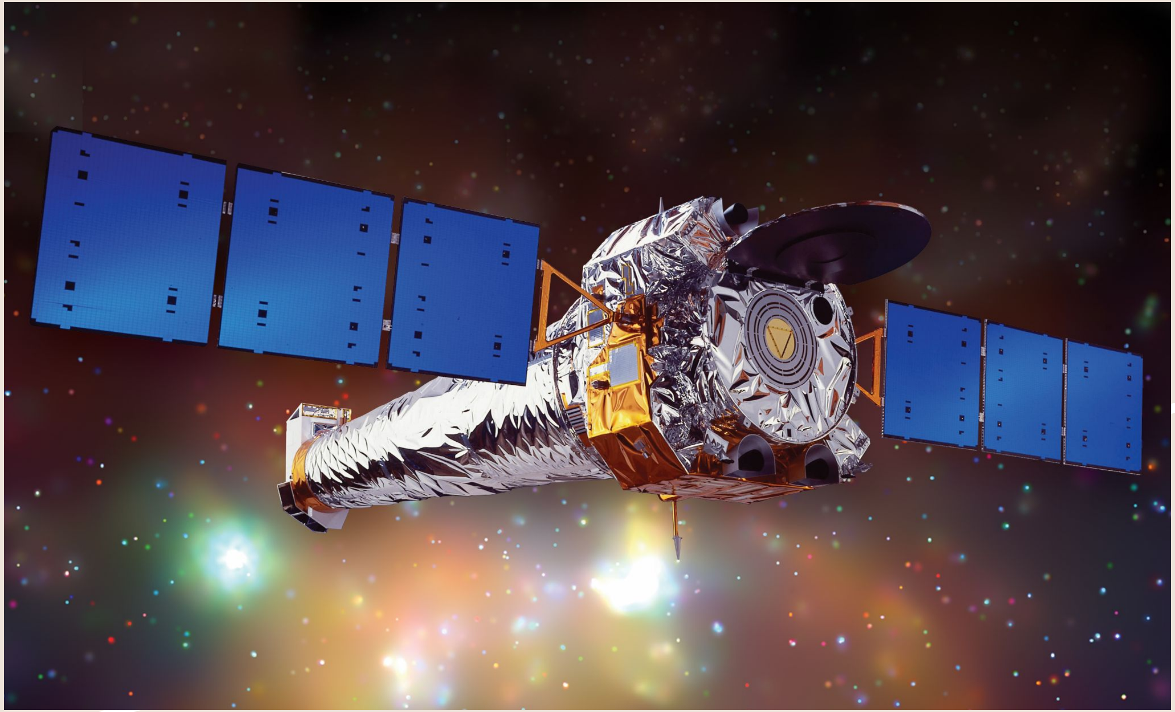

ACIS-I observations in 2001

Net count rate: 1.134x 10^{-2} cts/s

~450 photons within the source extraction region 5”

Chandra view of the active nucleus in NGC 3894

- source extraction region: 5” radius circle (white solid)
- background: annulus with 10” and 20” radii (white dashed)

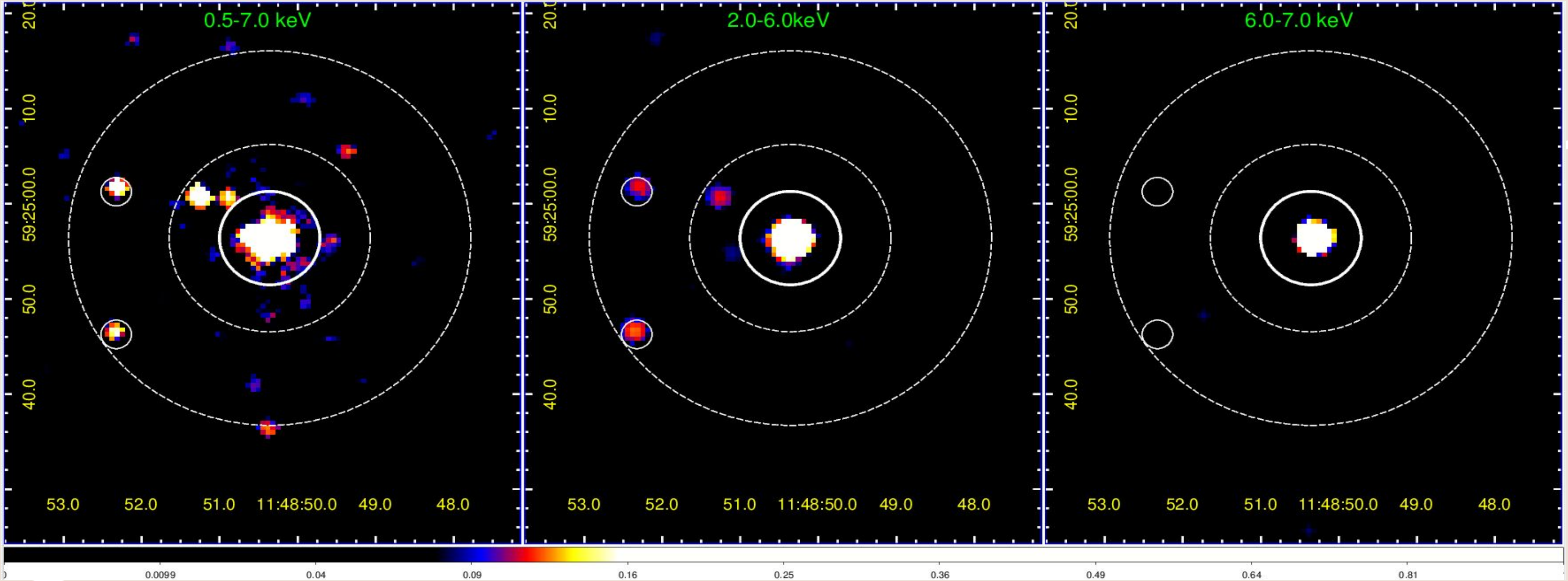

- excluding the two 2.5” radii circles corresponding to bright point sources (solid)
- Chandra images of NGC 3894, smoothed with 3 sigma; as shown, the 6-7 keV emission is restricted to the unresolved core

K.Balasubramaniam et al. to be submitted

Chandra 6-7 keV PSF profile

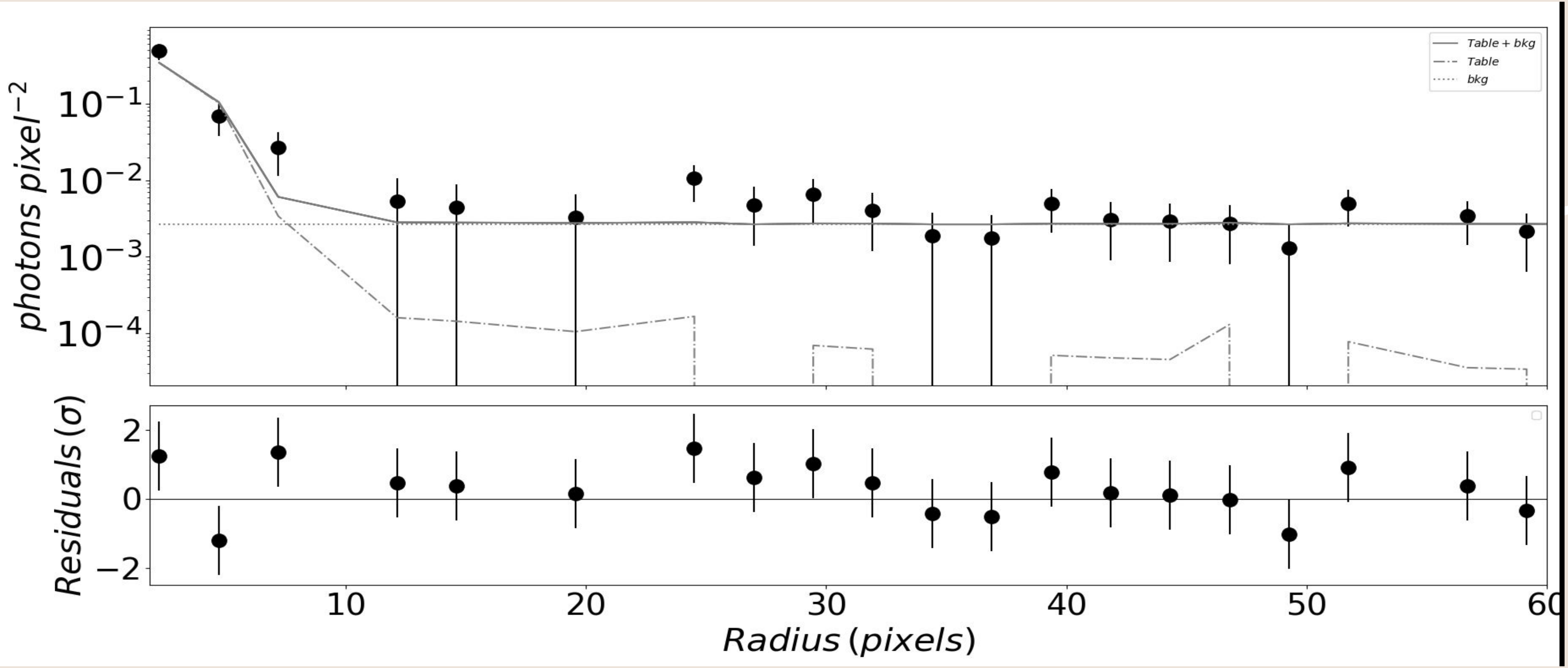

Indeed, no extension in the 6-7 keV emission beyond the PSF (simulated for the 6-7 keV range)

K.Balasubramaniam et al. to be submitted

X-ray hardness ratio analysis

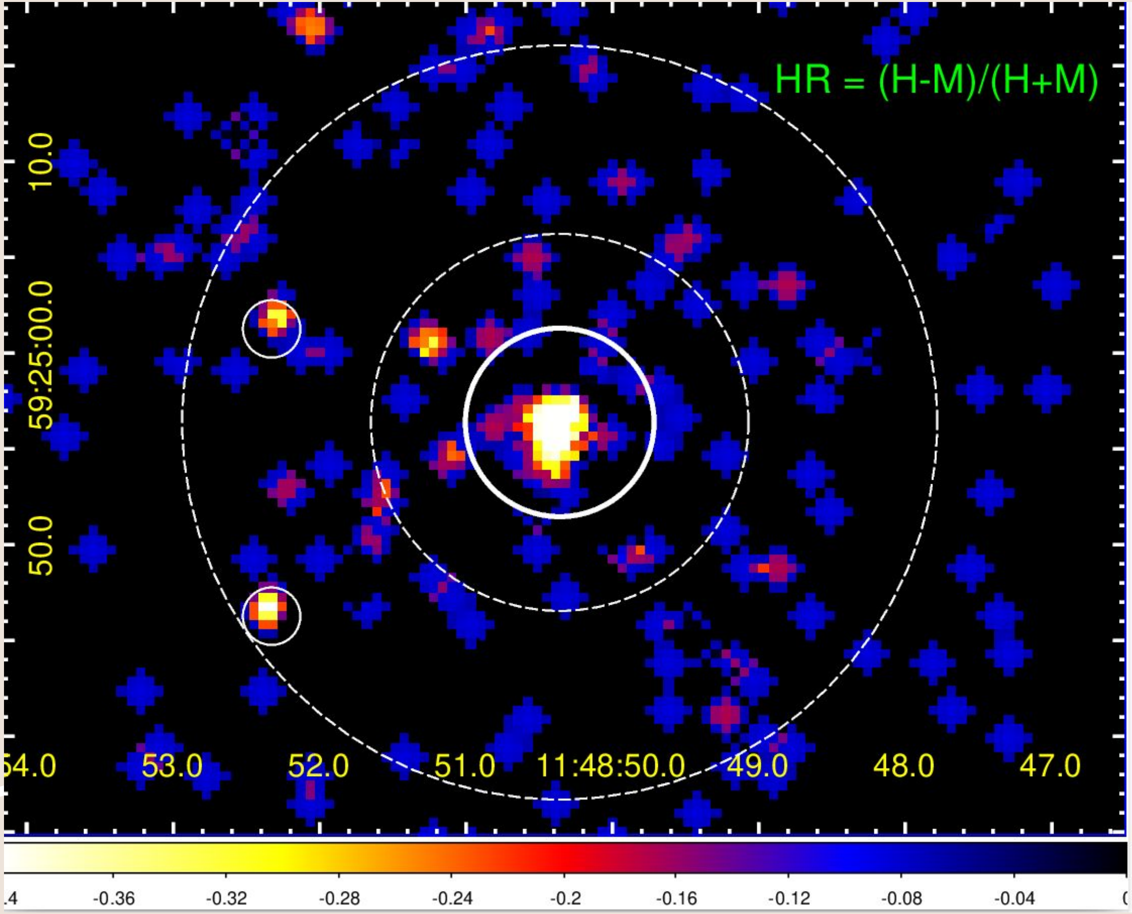

- Hardness ratio map HR=(H-M)/(H+M), between the Hard (6-7keV) and Medium (2-6keV) bands.
- Note the map is reliable with no prominent artefacts because the PSFs for both M and H bands are rather similar.

K.Balasubramaniam et al. to be submitted

Chandra spectral modelling

A simple model **phabs.gal * (zphabs*powerlaw + zapec)** applied to the background-subtracted source spectrum, returns a very flat, moderately absorbed power-law (N_H ~ 2e22cm^{-2}, Gamma ~ 1.3), contributed by a thermal component (kT ~ 0.8 keV; assumed solar metallicity). The residuals indicate however a presence of the emission lines, including

- A line around 6.4 keV, consistent with the neutral iron K-shell line;
- A line around 4.6 keV, which most likely is the instrumental artefact (Si escape peak, following the Fe 6.4 keV emission (see Grimm et al. 2009, ApJ, 690, 128)
- Positive residuals in the soft range (-> see next slides!)

Adding a simple redshifted Gaussian line component to the model:
phabs.gal *(zphabs*(powerlaw+zgauss) + zapec)
improves the fitting, and confirmed the presence of a neutral iron K-shell line with the EW ~ 0.6 keV.

Best fit parameters

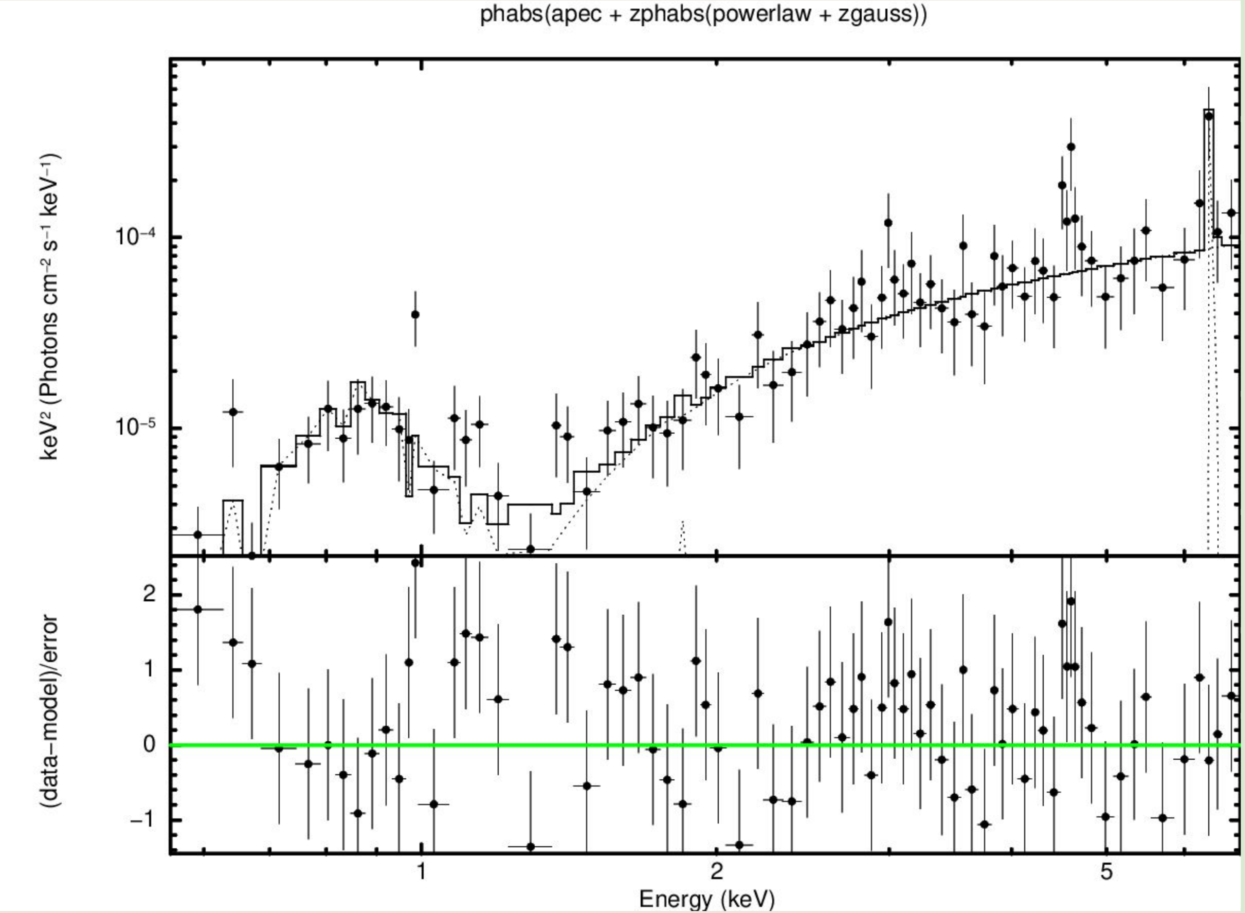

N_H (Gal) [cm^{-2}] (frozen!)	0.0183×10^{22}
kT [keV]	0.789 +/- 0.0579
N_H (int) [cm^{-2}]	(2.21 +/- 0.66) x 10^{22}
Γ_{src}	1.28 +/- 0.37
Line E [keV]	6.47 +/- 0.05
EW [keV]	0.6
Unabsorbed flux of the PL component (0.5-7.0) [$erg/cm^2/s$]	1.987×10^{-13}

K.Balasubramaniam et al. to be submitted

We considered more sophisticated emission models as well, however due to a rather limited photon statistics, those did not improve the fitting, or actually made it worse.

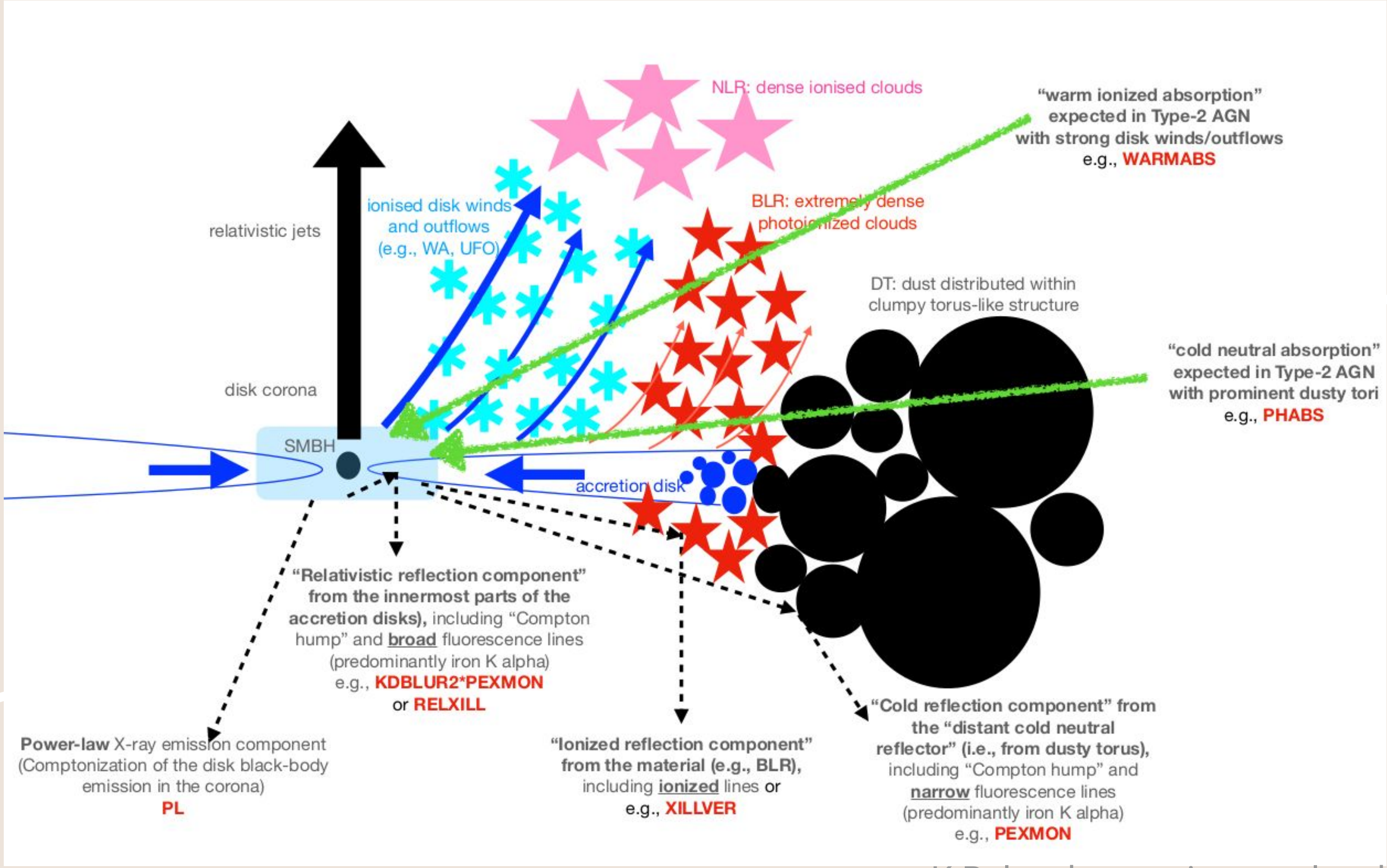

K.Balasubramaniam et al. to be submitted

- Positive residuals we see in the core spectrum of NGC 3894 in the soft range (<~ 1keV), may indicate the presence of the photoionized plasma component in addition to the collisionally ionized 0.8 keV plasma modeled here by apec, similarly as seen in PKS 1718−649

PKS 1718−649 - another very compact CSO with LINER-type nucleus, detected in gamma-rays

X-ray data analysis: Beuchert et al. 2018

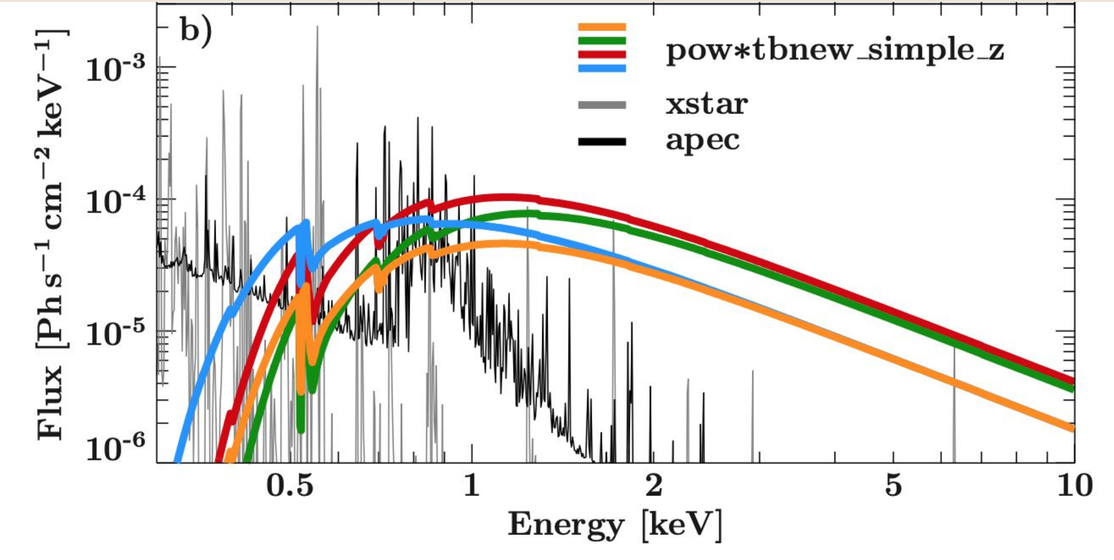

XMM-Newton
+ Multiple Chandra pointings

Model:
- photoionized plasma (xstar)
- collisionally ionized plasma (apec)
- absorbed PL (variable!)

Multiwavelength SED of NGC 3894

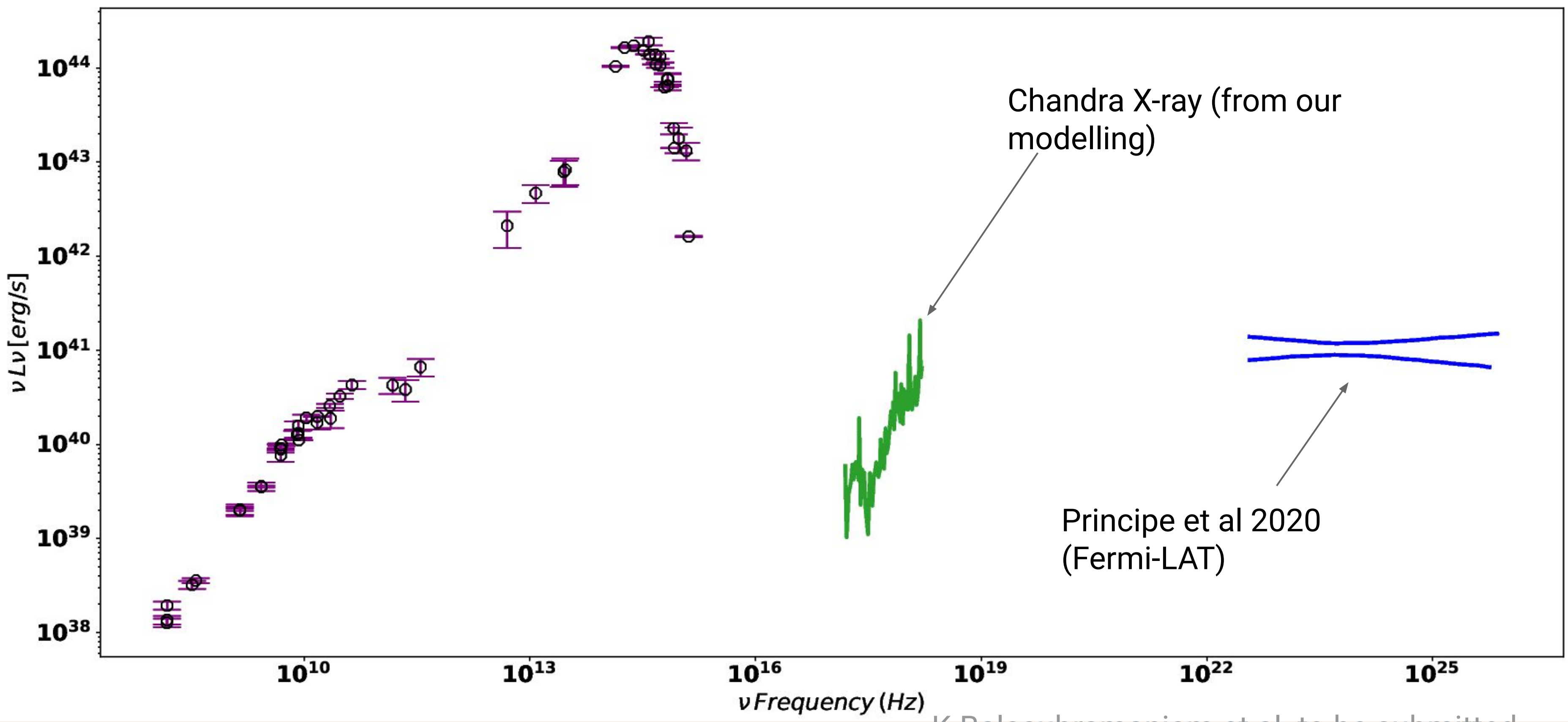

K.Balasubramaniam et al. to be submitted

Summary

- One of the youngest nearby radio galaxies; one of a few CSOs detected in gamma-rays by Fermi-LAT.
- Here we present the first attempt for detailed X-ray spectroscopy.

- Very flat PL with Gamma 1.3+/-0.3, and total luminosity L_X ~ 6e40erg/s.
- Neutral iron line at 6.4keV with relatively large EW ~0.6keV !!!
- Poor photon statistics makes fitting quite challenging although we believe that our findings regarding a very flat PL component and neutral iron line with relatively large EW, are robust!